Chemical Engineering Journal 450 (2022) 138047

Contents lists available at ScienceDirect

Chemical Engineering Journal

journal homepage: www.elsevier.com/locate/cej

Wet-slurry fabrication using PVdF-HFP binder with sulfide electrolytes via synergetic cosolvent approach for all-solid-state batteries

Kyu Tae Kim [a], Tae Young Kwon [a,b], Yong Bae Song [a], Sang-Mo Kim [c], Soon Chul Byun [c], Hong-Seok Min [c], Sa Heum Kim [c], Yoon Seok Jung [a,*]

[a] Department of Chemical and Biomolecular Engineering, Yonsei University, Seoul 03722, South Korea
[b] Department of Energy Engineering, Hanyang University, Seoul 04763, South Korea
[c] Hyundai Motor Company, Hwaseong-si, Gyeonggi-do 18280, Republic of Korea

ARTICLE INFO

Keywords:
Solid electrolytes
Solid-state batteries
Composite electrodes
Binders
Fluorinated polymers

ABSTRACT

Polymeric binders are a crucial component of large-format all-solid-state Li batteries (ASLBs) that employ sulfide solid electrolytes. However, the severe dissolution of sulfide solid electrolyte materials into conventional polar solvents restricts the suitability of slurry-processing solvents to less polar molecules, and in turn, the suitability of materials for polymeric binders to rubbers, such as nitrile butadiene rubber (NBR). In this study, a synergistic cosolvent approach is employed, to render poly(vinylidene fluoride-hexafluoropropylene) (PVdF-HFP), which is sulfide-slurry-incompatible, amenable to slurry fabrication. The synergistic combination of highly volatile ethyl acetate, and less volatile hexyl butyrate allows for the utilization of PVdF-HFP as it is soluble in the former but not in the latter, while avoiding the binder migration problem. A comparative investigation of sheet-type $LiNi_{0.70}Co_{0.15}Mn_{0.15}O_2$ electrodes comprising PVdF-HFP or NBR, demonstrates the superior performance of the former. Specifically, it is revealed that the effective volume fraction and binder distribution in the electrodes are key factors for determining the electrochemical performance. The advantageous features of PVdF-HFP over NBR are highlighted, particularly at a low temperature of 0 °C or under a low external operating pressure of 2 MPa. Finally, the encouraging performance of pouch-type $LiNi_{0.70}Co_{0.15}Mn_{0.15}O_2$/graphite ASLB full cells fabricated using PVdF-HFP, is successfully demonstrated.

1. Introduction

The remarkable progress in lithium-ion battery (LIB) technology has motivated the electrification of power trains with these energy sources [1,2]. However, its popularization has been hampered by safety concerns owing to the use of flammable organic liquid electrolytes and the limited energy density [3,4]. In this regard, solid-state batteries that utilize inorganic solid electrolytes (SEs) represent a potential breakthrough [5–9]. The development of several types of superionic conductors, including sulfides, such as $Li_{5.5}PS_{4.5}Cl_{1.5}$ [10]: 10 mS cm^{-1}; oxides, such as $Li_7La_3Zr_2O_{12}$ [11]: 0.1–1 mS cm^{-1}; halides, such as Li_3YX_6 (X = Cl, Br) [12,13]: 0.51–1.7 mS cm^{-1}; and closo-borates, such as $0.7Li(CB_9H_{10})$-$0.3Li(CB_{11}H_{12})$ [14,15]: 6.7 mS cm^{-1}, have provided options for constructing all-solid-state Li batteries (ASLBs) [10,12,16–21]. Specifically, sulfide materials exhibit outstanding properties of high ionic conductivities and mechanical sintering ability at room temperature, which are critical for the scalable fabrication of room temperature-operable ASLBs.

However, the fabrication technology for large-format ASLBs using sulfide SEs has remained in its infancy. Polymeric binders are crucial for the integration of all solid components in electrodes and/or in SE membranes for ASLBs [22–31]. While most lab-scale all-solid-state cells are tested under high external pressures of tens of megapascals, low pressures of a few megapascals are required for practical applications, at which the effects of polymeric binders become more significant [21,32–34]. The wet-slurry protocol is highly competitive for manufacturing polymeric binders, as it is applicable to well-established LIB manufacturing infrastructures [21,32,35–37]. However, the high reactivity of sulfide SEs with polar solvents restricts the range of suitable slurry-processing solvents, and in turn, that of polymeric binders [38–43]. Thus, non-polar or low-polarity organic solvents, such as xylene, and polymeric binders derived from rubber, such as butadiene rubber and nitrile butadiene rubber (NBR), have generally been used. Recently, the selection strategies for processing solvents, based on the

* Corresponding author.
E-mail address: yoonsjung@yonsei.ac.kr (Y.S. Jung).

https://doi.org/10.1016/j.cej.2022.138047
Received 2 May 2022; Received in revised form 16 June 2022; Accepted 9 July 2022
Available online 14 July 2022

polarity index, donor number, dipole moment, and steric effects, have suggested several favorable candidates, such as dibromomethane (DBM), hexyl butyrate (HB), benzyl acetate (BA), and anisole [38–41], however, little attention has been paid to their effects on binder distribution [25,38,40,41,44–47].

The use of poly(vinylidene fluoride) (PVdF), which has been validated in the LIB industry over the decades, has not been attempted for composite electrodes of the ASLB. An exception is the use of poly (vinylidene fluoride-hexafluoropropylene) (PVdF-HFP) in SE membranes [48,49]. Meanwhile, the use of SEs makes polymeric binders insulating in ASLBs [50]. This is distinctly different from LIBs, wherein binders are swollen by liquid electrolytes, and are thus Li^+ conductive [51,52]. Consequently, slurry-fabricated electrodes have shown far inferior electrochemical performances in ASLB cells compared to electrodes composed of simple mixture electrodes without binders [25]. The insulating properties of polymeric binders can be addressed by either endowing them with Li^+ conductivity [40,41,44,53] or by minimizing their content [39,54]. The latter can be achieved by the selection and development of novel binders with improved mechanical properties.

Recently, our group reported a slurry fabrication protocol using cosolvents and Li salts to introduce Li^+-conductive dry-polymer-electrolyte-based binders into ASLBs [40,41]. Two solvents, DBM and HB, operated synergistically not only to dissolve NBR and LiTFSI but also to control polymer dispersion without significantly disturbing the slurry protocol.

Based on this background and motivation, we report a slurry fabrication protocol using cosolvents to accommodate mechanically and electrochemically favorable PVdF-HFP binders in ASLBs for the first time. Volatile and polar EA dissolves PVdF-HFP, which is insoluble in known sulfide-compatible processing solvents, while non-volatile and less polar HB suppresses binder migration. Electrodes fabricated using PVdF-HFP binder and EA + HB cosolvents showed robust adhesion properties. Moreover, we demonstrate that the density and distribution of polymeric binders give rise to the considerable outperformance of the electrodes fabricated using PVdF-HFP, compared with those fabricated using conventional NBR.

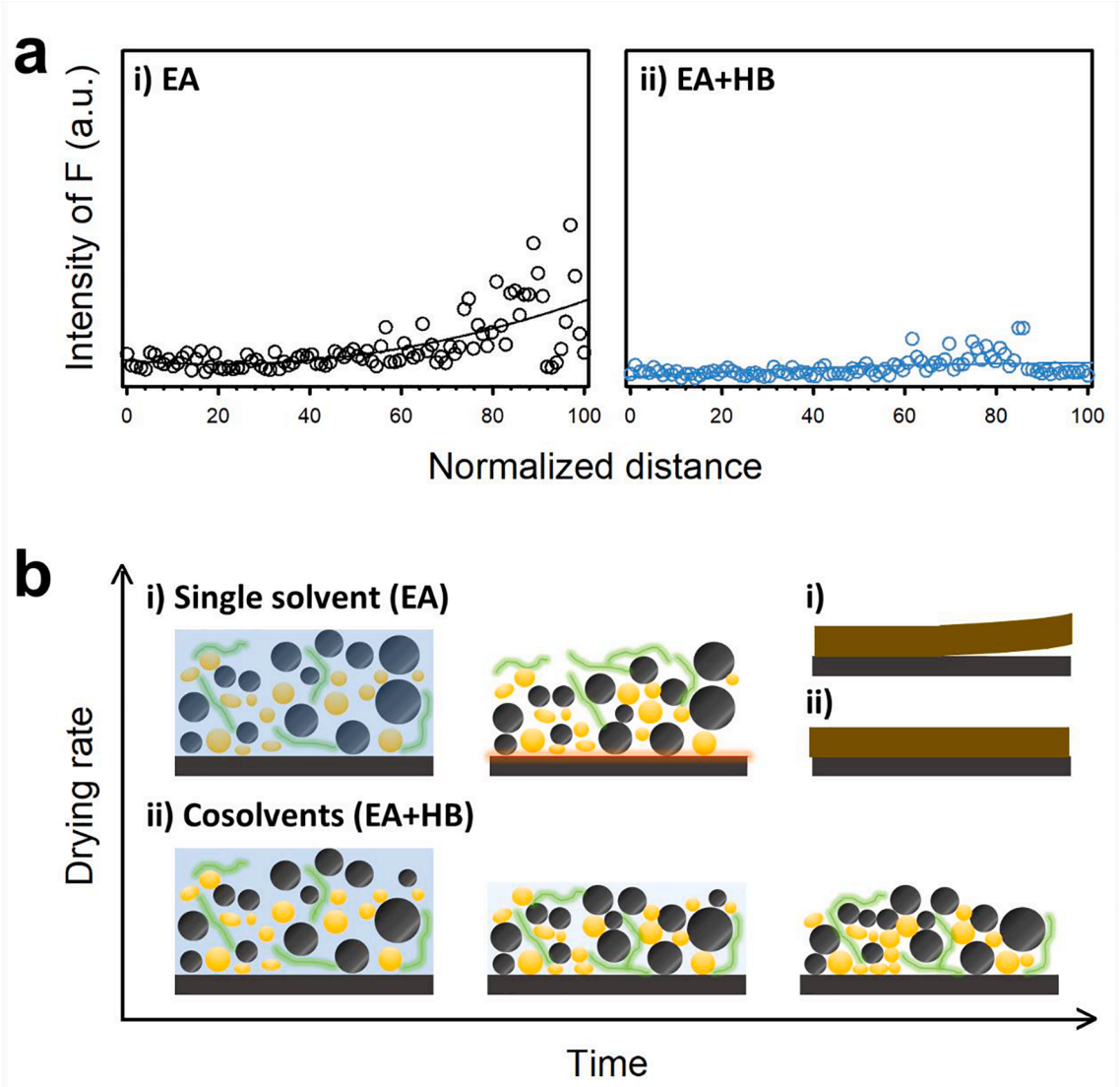

Fig. 1. Comparison of PVdF-HFP binder distribution in electrodes fabricated using EA as a single solvent and the EA + HB cosolvent. a) PVdF-HFP cross-sectional concentration in the Gr electrode prepared using i) EA and ii) EA + HB, determined based on EDXS F signals in Fig. S4. b) (i) Schematic illustrating the severe upward binder migration when highly volatile EA was used as a single solvent, resulting in poor adhesion of the electrode layers on the current collectors. (ii) Even binder distribution throughout the electrode depth in the electrodes fabricated using the EA + HB cosolvent.

2. Results and discussion

2.1. Compatibility and applicability of EA + HB cosolvents

The PVdF-HFP used in this study was calculated to have a number-average molecular weight (M_n) of 1.4 × 10^5 and an HFP fraction of 5.1 mol %, based on 400 MHz ^{19}F nuclear magnetic resonance analysis (Fig. S1) and gel permeation chromatography measurements (Table S1). EA was first selected as the processing solvent as PVdF-HFP is soluble (or dispersible) in it, as shown in Fig. S2, while the sulfide SE, $Li_6PS_5Cl_{0.5}Br_{0.5}$ (LPSX) remained intact. However, the $LiNi_{0.7}Co_{0.15}Mn_{0.15}O_2$ (NCM) electrodes fabricated using PVdF-HFP and EA as a single solvent exhibited poor adhesion to the current collector (Fig. S3a). Considering the high vapor pressure (10 kPa at 20 °C) and low boiling point (77 °C) of EA, the rapid evaporation of EA from slurries during the drying process causes binder migration, which leads to weak adhesion [46,55,56]. To address this issue, HB, a non-volatile and sulfide-compatible processing solvent (vapor pressure: 0.031 kPa at 20 °C, boiling point: 205 °C) [57], was introduced as a cosolvent. Consequently, the NCM electrodes fabricated using the EA + HB cosolvent showed robust adhesion (Fig. S3b).

Control experiments were performed to investigate the effectiveness of the EA + HB cosolvent on binder distribution. NCM electrodes were excluded because of their compositional complexity and poor mechanical properties resulting from the use of EA single solvents (Fig. S3a). Instead, two graphite (Gr) electrodes comprising PVdF-HFP with identical compositions (Gr:PVdF-HFP = 90:10 weight ratio) were prepared using EA or EA + HB. Fluorine was used as an indicator of the presence of PVdF-HFP in the Gr electrodes. Fig. 1a displays the cross-sectional concentration profile of F in Gr electrodes fabricated using EA or EA + HB, obtained by employing a field-emission scanning electron microscopy energy dispersive X-ray spectroscopy (FESEM-EDXS). The quantitative data are summarized in Table S2. The Gr electrodes fabricated using EA contained a higher concentration of PVdF-HFP at the top of the electrode (Fig. 1a (i)), whereas the F signals were evenly distributed throughout the electrode depth when EA + HB was used (Fig. 1a (ii)). Consistently, the corresponding cross-sectional FESEM images (Fig. S4) displayed an uneven distribution of pores in the electrode when EA was used and uniform pore distribution when EA + HB was utilized. These results confirmed that the use of EA + HB cosolvents is effective for suppressing binder migration and thus enhancing the mechanical integrity of the electrodes, as illustrated in Fig. 1b.

The compatibility of the EA + HB cosolvents with the sulfide SE of LPSX and its applicability to ASLBs were then assessed (Fig. 2). Fig. 2a shows the Li^+ conductivities of the LPSX samples before and after exposure to EA or EA + HB, measured by the AC impedance method using Ti/sample/Ti Li^+-blocking symmetric cells at 30 °C. When exposed to EA, the Li^+ conductivity of LPSX decreased from 4.5 to 2.8 mS cm^{-1} (62 % retention), which was attributed to the reactivity originating from the ester group in EA. The addition of HB to EA, EA + HB, significantly alleviated Li^+ conductivity attrition (3.7 mS cm^{-1}, 82 % retention). It is considered that, despite the presence of the same ester group in EA and HB, the reactivity of the ester group in HB is suppressed due to steric hindrance by the bulky hexyl group [41].

The electrochemical performances of the NCM/Li-In half cells at 30 °C for the NCM electrodes comprising PVdF-HFP fabricated using EA or EA + HB are presented in Fig. 2c and d. Due to the poor mechanical property of electrodes fabricated using EA, electrodes with low mass loading of ~ 4 mg cm^{-2} were prepared for both electrodes for fair comparison. The difference between the two electrodes were marginal: the first-cycle discharge capacity and initial Coulombic efficiency (ICE) were 163 mA h g^{-1} and 77.0 %, respectively, when only EA was used,

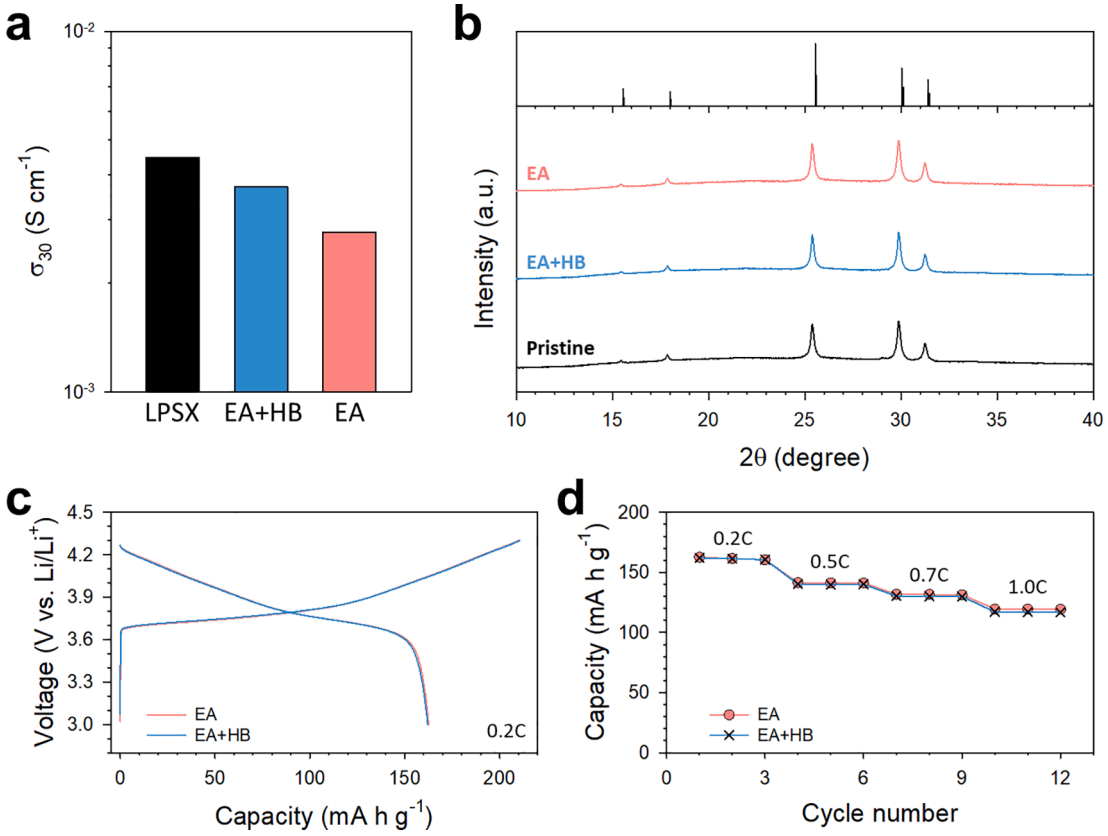

Fig. 2. Compatibility results of slurry-processing solvents for LPSX ($Li_6PS_5Cl_{0.5}Br_{0.5}$). a) Li^+ conductivities at 30 °C and b) XRD patterns for LPSX before and after exposure to EA or EA + HB. c) First-cycle charge-discharge voltage profiles at 0.2 C and 30 °C under 70 MPa for NCM/Li-In all-solid-state half cells employing NCM electrodes fabricated using EA or EA + HB, and d) the corresponding rate capabilities.

and 162 mA h g^{-1} and 77.5 %, respectively, when EA + HB were used. In addition, another EA-miscible solvent, BA, could be used as a cosolvent (Fig. S5). It should be noted that the type or ratio of cosolvents did not result in significant differences in the electrochemical performances.

2.2. The effect of binders on electrochemical performance

The effects of polymeric binders on the electrochemical performances of the ASLBs were investigated by comparing the performance of the NCM electrodes fabricated using PVdF-HFP with that of NBR-fabricated electrodes (Fig. 3). EA + HB were used as the processing solvents. Because the specific densities of PVdF-HFP and NBR differ significantly (1.77 vs 1.00 g cm^{-3}, respectively), a comparison should be made in terms of not only equivalent weight fractions but also equivalent volume fractions of the binders. NBR used at weight and volume fractions equivalent to those for PVdF-HFP are referred to as "NBR-wt" and "NBR-vol" (Table S3), respectively. When using binders with an equivalent weight fraction (2.5 wt%), the capacities of the PVdF-HFP NCM electrodes were substantially higher, compared to those achieved using NBR-wt electrodes (160 vs 149 mA h g^{-1} at 0.2 C for PVdF-HFP and NBR-wt electrodes, respectively, Fig. 3a, b). These results were predictable because each polymeric binder that blocks Li^+ conduction paths is present in a specific volume fraction in the electrodes. Not surprisingly, the NCM electrodes comprising PVdF-HFP and NBR-vol (with an equivalent volume ratio of 4.8 vol%) exhibited similar electrochemical performances (Fig. 3a, b). These results emphasize that the effective volume of polymeric binders for ASLBs is the key factor determining Li^+ contact resistance.

However, further electrochemical characterization results indicated overlooked differences among the three electrode samples. The NCM electrodes composed of NBR-vol showed a higher ICE (74.7 %) than those fabricated with NBR-wt (72.0 %) (Fig. 3c). This result could be attributed to the lower volume fraction of the insulating binder in NBR-vol (4.8 vol%), compared with that in NBR-wt (8.2 vol%) (Table S3). A larger fraction of insulating materials in composite electrodes reflects more severe electrochemo-mechanical degradation in terms of electrical contacts [25]. Furthermore, despite the identical volume fraction, the ICE of the PVdF-HFP NCM electrodes was higher (76.8 %) than the ICE of the NBR-vol counterparts (74.7 %). This result indicates the superiority of PVdF-HFP over NBR, partly explained by its higher electrochemical stability, as evidenced by the cyclic voltammetry results in Fig. S6. The transient discharge voltage profiles, obtained from galvanostatic intermittent titration technique (GITT) measurements, and the corresponding polarization curves are displayed in Fig. 3d. The distinctly lower capacity attained using NBR-wt, compared with those using NBR-vol or PVdF-HFP, agrees well with the results in Fig. 3a, b; however, it is notable that the polarization was lower in the case of PVdF-HFP than with NBR-vol. Electrochemical impedance spectroscopy (EIS) results followed the same trend as that of the GITT results (Fig. S7). The interfacial resistances, corresponding to the amplitudes of the semicircles, increased in the following order: PVdF-HFP < NBR-vol < NBR-wt. Furthermore, the Li^+ and e^- conductivities of the PVdF-HFP and NBR NCM electrodes, measured using (Li-In)/SE/electrode/SE/(Li-In) and Ti/electrode/Ti symmetric cells, respectively, are shown in Fig. 3e-g, S8, and Table S4. The Li^+ conductivities of the electrodes followed the electrochemical performance trends (PVdF-HFP ≈ NBR-vol

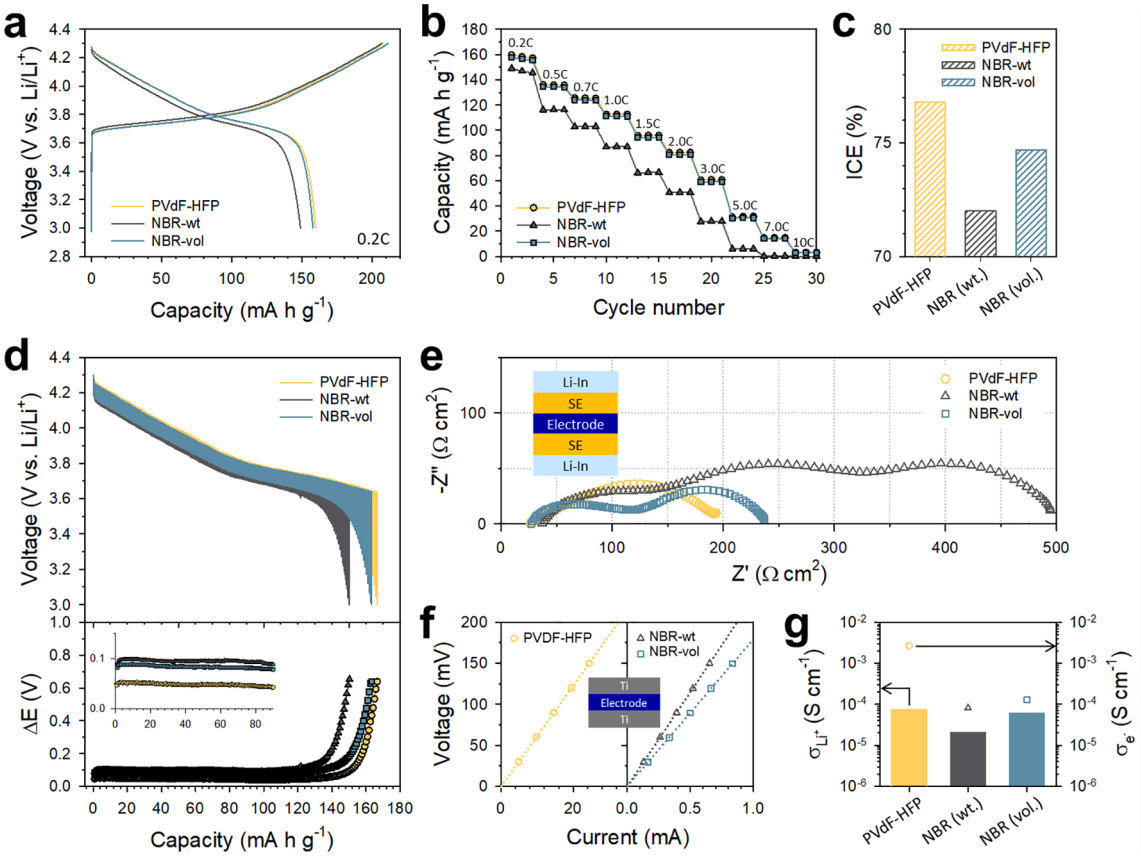

Fig. 3. Comparative electrochemical characterization of sheet-type NCM electrodes fabricated from slurries using PVdF-HFP, NBR-wt (the same weight fraction as PVdF-HFP, 2.5 wt%) and NBR-vol (the same volume fraction as PVdF-HFP, 4.8 vol%): a) First-cycle charge-discharge voltage profiles of NCM electrodes at 0.2 C and 30 °C, and the corresponding b) rate capabilities and c) ICEs (initial Coulombic efficiencies). d) Transient discharge voltage profiles and the corresponding polarization curves obtained employing GITT. e) Nyquist plots of e^--blocking (Li-In)/LPSX/electrode/LPSX/(Li-In) symmetric cells and f) i-V curves obtained from Li^+-blocking Ti/electrode/Ti symmetric cells and g) the resulting Li^+ (left) and e^- (right) conductivities. All cells were tested under 70 MPa.

> NBR-wt). However, unexpected results were obtained for the e^- conductivities, descending in the order of PVdF-HFP ≫ NBR-vol > NBR-wt; this is discussed later.

In summary, the PVdF-HFP electrodes outperformed those comprising an equivalent weight fraction of NBR (NBR-wt) due to the smaller volume fraction of PVdF-HFP than that of NBR-wt. However, the better performance of PVdF-HFP electrodes compared to that of electrodes comprising NBR-vol, observed in the ICEs, and the GITT and EIS results, is intriguing.

To explain the difference in performance between the PVdF-HFP and NBR-vol electrodes, the spatial distribution of the binder should be considered [58]. Thus, control experiments for the two NCM electrodes composed of PVdF-HFP and NBR-vol were conducted. The corresponding FESEM images are displayed in Fig. 4a–f. In the case of PVdF-HFP, the binder was distributed evenly throughout the electrode as uniform films (Fig. 4a, b). In contrast, for NBR, the binder was concentrated around the NCM particles in an irregular lumpy form (Fig. 4d, e). In the large-scale images shown in Fig. 4c and f, no visible cracks were observed for the PVdF-HFP NCM electrodes, whereas the NBR-vol electrodes exhibited noticeable cracks at the microscale. It is speculated that the polar –CN group in NBR facilitates binder adsorption onto the NCM surfaces, which leads to a concentrated distribution of NBR around NCM [58]. Accordingly, interfacial ionic and electronic conduction would be severely obstructed [25]. Thus, the performance difference determined by the binder, despite the equivalent volume fraction, could be understood.

To further investigate the different performances varied with the type of binder, electrochemical performances of the NCM electrodes using PVdF-HFP or NBR-vol were evaluated at lower temperatures of 0 and 10 °C (Fig. 4g, h). Nyquist plots at different temperatures in Fig. 4g showed the remarkable increase of the semicircle amplitudes, as lowering the temperature, indicating the increasing interfacial resistances. By fitting the Nyquist plots using an equivalent circuit model (Fig. S9a), the intercept values and the semicircle amplitudes that correspond to the resistances of the SE separating layer and the interfacial resistance, respectively, were extracted (Fig. S9b), and corresponding Arrhenius plots are displayed in Fig. S9c, d. Notably, the activation energies for the interfacial resistance (R2, 0.65 and 0.62 eV for using PVDF-HFP and NBR, respectively) were much higher, compared with those for the SE layer resistance (R1, 0.18 eV and 0.19 eV for using PVDF-HFP and NBR, respectively), indicating much higher contribution of the interfacial resistance at lower temperature. Nyquist plots at elevated temperatures of 40, 50, and 60 °C are also provided in Fig. S10. Consistent with the EIS results at 0 °C (Fig.. 4 g), the NCM electrodes made of PVDF-HFP clearly showed the lower overpotential and correspondingly larger capacities at 0 °C, compared with those made of NBR-vol (Fig. 4h). The inferior performance of the NCM electrodes using NBR-vol to those for using PVDF-HFP, revealed at 0 °C thus far, is rooted in the concentrated distribution of binders, which obstructs the interfacial Li^+ and e^- conduction. The latter is supported by the over an order of magnitude higher e^- conductivity of the NCM electrodes using PVDF-HFP than those for using NBR-vol (2.7×10^{-3} vs 1.3×10^{-4} S cm^{-1}, Fig. 3g).

As the effects of binders become more pronounced at lower operating pressure, NCM electrodes made of PVDF-HFP or NBR-vol were also tested under the practically-acceptable operating pressure of 2 MPa [21], and the corresponding results are shown in Fig. 4i–l. The similar capacities at the high operating pressure of 70 MPa became distinctly different at the low operating pressure of 2 MPa, especially at higher C-rates (91.3 vs 71.5 mA h g^{-1} at 1C for using PVDF-HFP and NBR-vol, respectively).

2.3. Practical evaluation

Finally, the practical applicability of PVdF-HFP was evaluated in NCM/Gr all-solid-state full cells (Fig. 5). PVdF-HFP could also be successfully applied to sheet-type Gr electrodes. The PVdF-HFP Gr electrodes outperformed the NBR-vol Gr electrodes (Fig. S11). Pellet-type NCM/Gr full cells fabricated using PVdF-HFP electrodes exhibited an initial discharge capacity of 160 mA h g_{NCM}^{-1} at 0.2 C, which was consistent with the results obtained for the NCM/Li-In half cells (Fig. 5a, S13a). NCM and Gr electrodes with the thickness of 67 and 66 μm, respectively, exhibited intimate contacts with SE layers (Fig. S12). In addition, they showed excellent capacity retention (93.2 %) at the 200th cycle, compared with the capacity at the 4th cycle. Finally, pouch-type NCM/Gr all-solid-state full cells were assembled and tested at 30 °C without externally applied pressure (Fig. 5b, S13b). Consistent with the results for the pellet-type cells, the pouch-type ASLBs displayed a first-cycle discharge capacity of 169 mA h g_{NCM}^{-1} at 0.1 C, highlighting the adaptability of the PVdF-HFP-based protocol for practical applications.

3. Conclusions

In summary, PVdF-HFP binders were successfully adapted to sheet-type electrodes for ASLBs using the cosolvent approach. EA was favorable for dissolving PVdF-HFP while the sulfide SEs remained relatively intact, but was not applicable for slurry fabrication as it is highly volatile, causing severe binder migration in the electrodes. This problem was resolved by adding HB as a cosolvent because it could not disperse PVdF-HFP but was less volatile and compatible with the sulfide SE. Thus, the electrodes comprising PVdF-HFP, tailored using the EA + HB cosolvent, did not suffer from binder migration and showed acceptable mechanical properties. Compared with the conventional binder for sulfide-electrolyte-based ASLBs, NBR, the higher specific density of PVdF-HFP allowed the reduction in the effective binder volume fraction in the electrodes, and the use of PVdF-HFP led to enhanced electrochemical performances when the suitability of the two binders was compared at equivalent weight fractions. Furthermore, it was demonstrated that NBR, bearing a highly polar –CN group, was selectively concentrated around the NCM particles and obstructed ionic and electronic conduction in the electrodes. In contrast, PVdF-HFP was distributed evenly throughout the electrodes. These differences in binder distribution resulted in the PVdF-HFP binders being more suitable for ASLB electrodes, especially at low temperatures or under low external operating pressures. Finally, NCM/Gr full cells exhibited good electrochemical performances with high capacities and stable capacity retention. The results of this study represent a significant contribution toward realizing practical all-solid-state technology and provide important insights into the design of polymeric binders amenable to slurry fabrication at the molecular scale.

4. Experimental section

Preparation of Materials: Argyrodite $Li_6PS_5Cl_{0.5}Br_{0.5}$ (LPSX) was prepared employing ball-milling and subsequent heat treatment under an Ar atmosphere. Thus, a stoichiometric mixture of Li_2S (99.9 %, Alfa-Aesar), P_2S_5 (99 %, Sigma Aldrich), and LiCl (99.99 %, Sigma Aldrich) was ball-milled at 600 rpm for 10 h in a ZrO_2 vial with ZrO_2 balls using a Pulverisette 7PL (Fritsch GmbH), followed by heat treatment at 550 °C for 5 h under an Ar atmosphere. The Li^+ conductivity of the resulting powder was 4.5 mS cm^{-1} at 30 °C. NCM powders coated with $LiNbO_3$ were used in this study. To prepare PVdF-HFP/(EA + HB) and NBR/(EA + HB) solutions, PVdF-HFP and NBR were first dissolved in EA (99.8 %, anhydrous, Sigma Aldrich), followed by the addition of HB (98 %, Sigma Aldrich). For the solvent compatibility tests, 100 mg of LPSX was immersed in each solvent (3.0 mL of EA or 3.0 mL of EA + HB (vol. ratio)), followed by removal of the solvents at 150 °C for 6 h under vacuum. All the liquids (EA and HB) and solids (PVdF-HFP and NBR) used for the slurries were dried using molecular sieves (4 Å, DAEJUNG) and at 100 °C under vacuum.

Electrode Fabrication: Wet slurries consisting of active materials (NCM or Gr), LPSX, polymeric binders (PVdF-HFP or NBR), and carbon

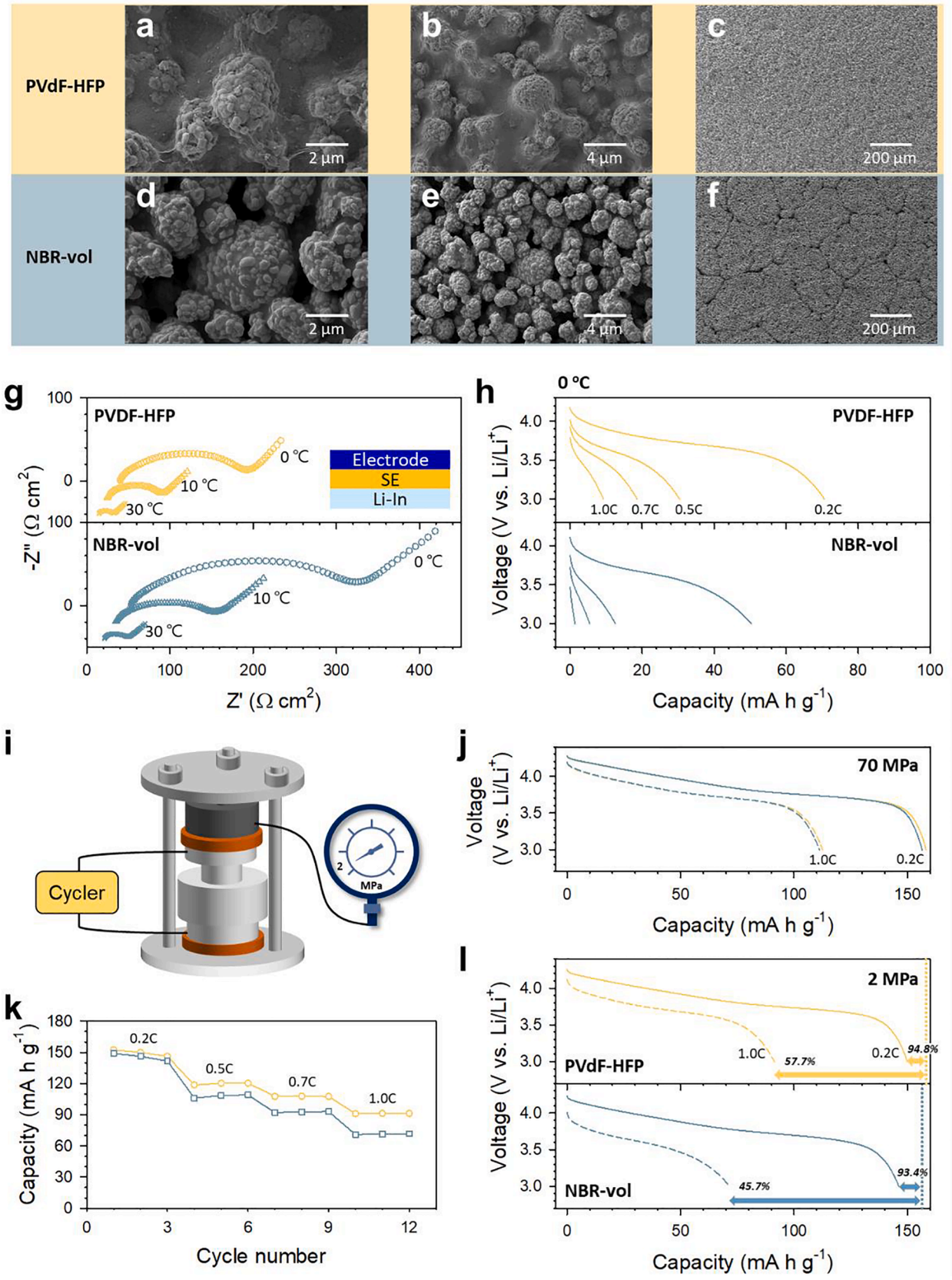

Fig. 4. Comparative characterization of NCM electrodes fabricated using PVdF-HFP and NBR-vol. FESEM images of NCM electrodes (without using SEs) fabricated using (a–c) PVdF-HFP and (d–f) NBR-vol. g) Nyquist plots of NCM/Li-In half cells recorded at 30, 10, and 0 °C. The data were obtained after 10 cycles. h) Discharge voltage profiles of NCM/Li-In half cells at 0 °C under 70 MPa. i) Schematic illustrating all-solid-state cells operated under a low external pressure of 2 MPa. j) Discharge voltage profiles of NCM/Li-In half cells at 30 °C, operated under the conventional high external pressure of 70 MPa. k) Rate capabilities and l) discharge voltage profiles of NCM/Li-In half cells at 30 °C, operated under a low external pressure of 2 MPa.

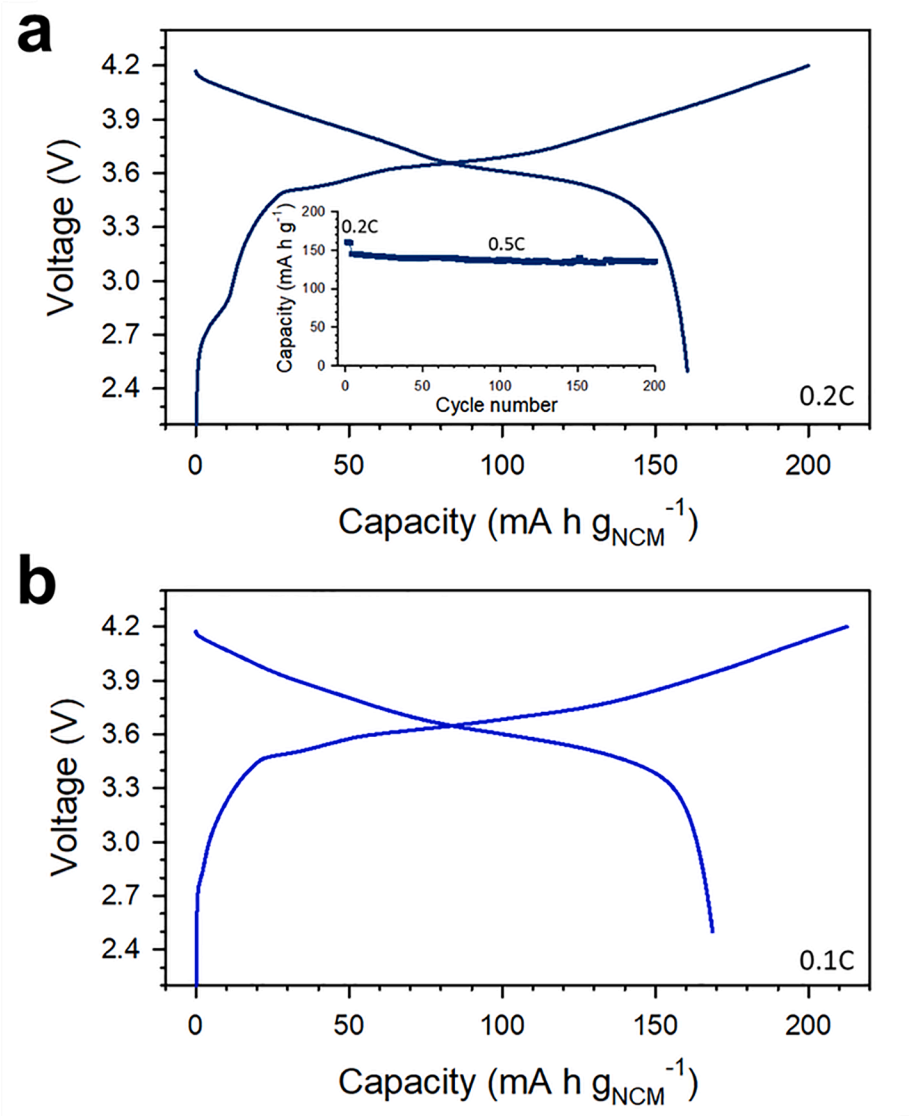

Fig. 5. Results at 30 °C for NCM/Gr all-solid-state full cells employing electrodes comprising the PVdF-HFP binder. a) First-cycle charge-discharge voltage profiles of pellet-type full cells at 0.2 C. The corresponding cycling performance at 0.2 C for the first four cycles and 0.5C for the subsequent cycles is shown in the inset. b) First-cycle charge-discharge voltage profiles of 15 × 20 mm^2 pouch-type full cells at 0.1 C.

additives (Super C65) were prepared to target compositions using EA + HB cosolvents. The electrode composition (weight ratio) was 75.0:21.0:2.5:1.5, and 60:36:2:2 for the NCM and Gr electrodes, respectively. For the NCM electrode comprising NBR at an equivalent volume fraction, the electrode composition was 75.82:21.23:1.52:1.43. The slurry mixtures were cast on current collectors (carbon-coated Al and Ni foils for the NCM and Gr electrodes, respectively) using the doctor-blade method, followed by heat treatment at 150 °C under vacuum. The mass loadings of NCM and Gr electrodes were 17.5 and 12.5 mg cm^{-2}, respectively. To characterize the PVdF-HFP distribution in the Gr electrode, wet slurries consisting of Gr and PVdF-HFP were prepared using EA or EA + HB. The electrode composition was 90:10. The slurry mixtures were cast on Ni foils, followed by heat treatment at 60 °C and 150 °C when using EA and EA + HB, respectively. To determine the PVdF-HFP and NBR distribution in the NCM electrodes, wet slurries consisting of NCM and the polymeric binders were prepared using EA + HB with target compositions of 95:5 and 97.1:2.9 in the case of PVdF-HFP and NBR, respectively.

Material Characterization: Cross-sections of the Gr electrodes were obtained by polishing at 6 kV for 6 h, followed by 4 kV for 3 h using an Ar ion beam (JEOL, IB19510CP). The corresponding FESEM images and EDXS data were acquired using an AURIGA (Carl ZEISS). To assess the reactivity between LPSX and solvents, 100 mg of LPSX were immersed in 3 mL of each solvent. The mixtures were stirred at 2000 rpm for 5 min and dried at 150 °C for 6 h. For the XRD measurements, the samples were sealed with a beryllium window and mounted on a MiniFlex 600 diffractometer (Rigaku Corp.; Cu Kα radiation of 1.5406 Å) at 40 kV and 15 mA. For ^{19}F nuclear magnetic resonance (NMR) spectroscopy, 80 mg of PVdF-HFP was dissolved in 600 μL of acetone-d_6 solvent and analyzed using an AVANCE III HD 400 (Bruker) [59]. The ^{19}F NMR spectra were fitted using MestReNova software. For gel permeation chromatography measurements, PVdF-HFP was diluted in dimethylformamide and analyzed using an Ultimate 3000 instrument (Thermo Fisher Scientific).

Electrochemical Characterization: The Li-In (nominal composition: $Li_{0.5}In$) electrodes, which were used as the counter and reference electrodes were prepared by ball-milling In (Sigma Aldrich, 99 %) and Li (FMC Lithium Corp.) powders. To fabricate the NCM (or Gr)/Li-In half cells, the electrodes and Li-In electrodes were placed on each side of the

pre-pelletized LPSX layers (150 mg) and pelletized at 370 MPa at room temperature. All procedures were conducted in a polyaryletheretherketone (PEEK) mold (1.3 cm^2) with two Ti metal rods. Galvanostatic charge–discharge cycling tests were performed at 30 or 0 °C between 3.0 and 4.3 V (vs Li/Li^+) for the NCM electrodes and between 0.005 and 2.000 V (vs Li/Li^+) for the Gr electrodes. The pellet-type NCM/Gr full cells were fabricated using the same procedure as that for the half cells, except that Gr was used instead of Li-In. To fabricate pouch-type NCM/Gr full cells, ~150 μm SE films were prepared as described in our previous study [60]. The electrodes and SE films were stacked and packed into a laminate bag. The laminated bag was sealed under vacuum and pressurized with isotactic pressing at 450 MPa. Galvanostatic charge–discharge cycling tests for the full cells were conducted at 30 °C between 3.0 and 4.2 V. The pellet-type all-solid-state cells were tested at pressures of 70 or 2 MPa. Pouch-type cells were tested under no external pressure. The EIS data were collected at an amplitude of 14.1 mV and frequency range from 10 mHz to 7 MHz using an Iviumstat (IVIUM Technologies Corp.). The GITT measurements were performed by applying a pulse current of 0.5 C for 60 s and rest for 2 h.

Declaration of Competing Interest

The authors declare that they have no known competing financial interests or personal relationships that could have appeared to influence the work reported in this paper.

Data availability

Data will be made available on request.

Acknowledgements

This work was supported by Hyundai Motor Company, by the National Research Foundation of Korea (NRF) funded by the Ministry of Science and ICT (NRF-2022M3J1A1085397), by the Technology Innovation Program (20007045) funded By the Ministry of Trade, Industry & Energy (MOTIE), and by the Yonsei University Research Fund of 2021 (2021-22-0326).

Appendix A. Supplementary data

Supplementary data to this article can be found online at https://doi.org/10.1016/j.cej.2022.138047.

References

[1] J.W. Choi, D. Aurbach, Promise and reality of post-lithium-ion batteries with high energy densities, Nat. Rev. Mater. 1 (2016) 16013, https://doi.org/10.1038/natrevmats.2016.13.
[2] X. Zeng, M. Li, D. Abd El-Hady, W. Alshitari, A.S. Al-Bogami, J. Lu, K. Amine, Commercialization of Lithium Battery Technologies for Electric Vehicles, Adv. Energy Mater. 9 (2019) 1900161, https://doi.org/10.1002/aenm.201900161.
[3] M. Li, J. Lu, Z. Chen, K. Amine, 30 Years of Lithium-Ion Batteries, Adv. Mater. 30 (2018) 1800561, https://doi.org/10.1002/adma.201800561.
[4] R. Schmuch, R. Wagner, G. Hörpel, T. Placke, M. Winter, Performance and cost of materials for lithium-based rechargeable automotive batteries, Nat. Energy 3 (2018) 267–278, https://doi.org/10.1038/s41560-018-0107-2.
[5] J. Janek, W.G. Zeier, A solid future for battery development, Nat. Energy 1 (2016) 16141, https://doi.org/10.1038/nenergy.2016.141.
[6] K.H. Park, Q. Bai, D.H. Kim, D.Y. Oh, Y. Zhu, Y. Mo, Y.S. Jung, Design Strategies, Practical Considerations, and New Solution Processes of Sulfide Solid Electrolytes for All-Solid-State Batteries, Adv. Energy Mater. 8 (2018) 1800035, https://doi.org/10.1002/aenm.201800035.
[7] T. Famprikis, P. Canepa, J.A. Dawson, M.S. Islam, C. Masquelier, Fundamentals of inorganic solid-state electrolytes for batteries, Nat. Mater. 18 (2019) 1278–1291, https://doi.org/10.1038/s41563-019-0431-3.
[8] Q. Zhao, S. Stalin, C.-Z. Zhao, L.A. Archer, Designing solid-state electrolytes for safe, energy-dense batteries, Nat. Rev. Mater. 5 (2020) 229–252, https://doi.org/10.1038/s41578-019-0165-5.
[9] Y.-G. Lee, S. Fujiki, C. Jung, N. Suzuki, N. Yashiro, R. Omoda, D.-S. Ko, T. Shiratsuchi, T. Sugimoto, S. Ryu, J.H. Ku, T. Watanabe, Y. Park, Y. Aihara, D. Im, I.T. Han, High-energy long-cycling all-solid-state lithium metal batteries enabled by silver–carbon composite anodes, Nat. Energy 5 (2020) 299–308, https://doi.org/10.1038/s41560-020-0575-z.
[10] H.-J. Deiseroth, S.-T. Kong, H. Eckert, J. Vannahme, C. Reiner, T. Zaiß, M. Schlosser, Li_6PS_5X: A Class of Crystalline Li-Rich Solids With an Unusually High Li^+ Mobility, Angew. Chem. Int. Ed. 47 (2008) 755–758, https://doi.org/10.1002/anie.200703900.
[11] S. Stramare, V. Thangadurai, W. Weppner, Lithium Lanthanum Titanates: A Review, Chem. Mater. 15 (2003) 3974–3990, https://doi.org/10.1021/cm0300516.
[12] T. Asano, A. Sakai, S. Ouchi, M. Sakaida, A. Miyazaki, S. Hasegawa, Solid Halide Electrolytes with High Lithium-Ion Conductivity for Application in 4 V Class Bulk-Type All-Solid-State Batteries, Adv. Mater. 30 (2018) 1803075, https://doi.org/10.1002/adma.201803075.
[13] H. Kwak, S. Wang, J. Park, Y. Liu, K.T. Kim, Y. Choi, Y. Mo, Y.S. Jung, Emerging Halide Superionic Conductors for All-Solid-State Batteries: Design, Synthesis, and Practical Applications, ACS Energy Lett. (2022) 1776–1805, https://doi.org/10.1021/acsenergylett.2c00438.
[14] L. Duchêne, D.H. Kim, Y.B. Song, S. Jun, R. Moury, A. Remhof, H. Hagemann, Y. S. Jung, C. Battaglia, Crystallization of closo-borate electrolytes from solution enabling infiltration into slurry-casted porous electrodes for all-solid-state batteries, Energy Storage Mater. 26 (2020) 543–549, https://doi.org/10.1016/j.ensm.2019.11.027.
[15] S. Kim, H. Oguchi, N. Toyama, T. Sato, S. Takagi, T. Otomo, D. Arunkumar, N. Kuwata, J. Kawamura, S.-I. Orimo, A complex hydride lithium superionic conductor for high-energy-density all-solid-state lithium metal batteries, Nat. Commun. 10 (2019) 1081, https://doi.org/10.1038/s41467-019-09061-9.
[16] A. Sakuda, A. Hayashi, M. Tatsumisago, Sulfide Solid Electrolyte with Favorable Mechanical Property for All-Solid-State Lithium Battery, Sci. Rep. 3 (2013) 2261, https://doi.org/10.1038/srep02261.
[17] F. Han, Y. Zhu, X. He, Y. Mo, C. Wang, Electrochemical Stability of Li10GeP2S12 and Li7La3Zr2O12 Solid Electrolytes, Adv. Energy Mater. 6 (2016) 1501590, https://doi.org/10.1002/aenm.201501590.
[18] J. Awaka, N. Kijima, H. Hayakawa, J. Akimoto, Synthesis and structure analysis of tetragonal Li7La3Zr2O12 with the garnet-related type structure, J. Solid State Chem. 182 (2009) 2046–2052, https://doi.org/10.1016/j.jssc.2009.05.020.
[19] J. Xu, L. Liu, N. Yao, F. Wu, H. Li, L. Chen, Liquid-involved synthesis and processing of sulfide-based solid electrolytes, electrodes, and all-solid-state batteries, Mater. Today Nano 8 (2019), 100048, https://doi.org/10.1016/j.mtnano.2019.100048.
[20] X. Li, J. Liang, X. Yang, K.R. Adair, C. Wang, F. Zhao, X. Sun, Progress and perspectives on halide lithium conductors for all-solid-state lithium batteries, Energy Environ. Sci. 13 (2020) 1429–1461, https://doi.org/10.1039/C9EE03828K.
[21] C. Wang, J. Liang, Y. Zhao, M. Zheng, X. Li, X. Sun, All-solid-state lithium batteries enabled by sulfide electrolytes: from fundamental research to practical engineering design, Energy Environ. Sci. 14 (2021) 2577–2619, https://doi.org/10.1039/D1EE00551K.
[22] S. Ito, S. Fujiki, T. Yamada, Y. Aihara, Y. Park, T.Y. Kim, S.-W. Baek, J.-M. Lee, S. Doo, N. Machida, A rocking chair type all-solid-state lithium ion battery adopting Li_2O–ZrO_2 coated $LiNi_{0.8}Co_{0.15}Al_{0.05}O_2$ and a sulfide based electrolyte, J. Power Sources 248 (2014) 943–950, https://doi.org/10.1016/j.jpowsour.2013.10.005.
[23] J.M. Whiteley, P. Taynton, W. Zhang, S.-H. Lee, Ultra-thin Solid-State Li-Ion Electrolyte Membrane Facilitated by a Self-Healing Polymer Matrix, Adv. Mater. 27 (2015) 6922–6927, https://doi.org/10.1002/adma.201502636.
[24] A. Sakuda, K. Kuratani, M. Yamamoto, M. Takahashi, T. Takeuchi, H. Kobayashi, All-Solid-State Battery Electrode Sheets Prepared by a Slurry Coating Process, J. Electrochem. Soc. 164 (2017) A2474–A2478, https://doi.org/10.1149/2.0951712jes.
[25] Y.J. Nam, D.Y. Oh, S.H. Jung, Y.S. Jung, Toward practical all-solid-state lithium-ion batteries with high energy density and safety: Comparative study for electrodes fabricated by dry- and slurry-mixing processes, J. Power Sources 375 (2018) 93–101, https://doi.org/10.1016/j.jpowsour.2017.11.031.
[26] N. Riphaus, P. Strobl, B. Stiaszny, T. Zinkevich, M. Yavuz, J. Schnell, S. Indris, H. A. Gasteiger, S.J. Sedlmaier, Slurry-Based Processing of Solid Electrolytes: A Comparative Binder Study, J. Electrochem. Soc. 165 (2018) A3993–A3999, https://doi.org/10.1149/2.0961816jes.
[27] M. Yamamoto, Y. Terauchi, A. Sakuda, A. Kato, M. Takahashi, Effects of volume variations under different compressive pressures on the performance and microstructure of all-solid-state batteries, J. Power Sources 473 (2020), 228595, https://doi.org/10.1016/j.jpowsour.2020.228595.
[28] T. Ates, M. Keller, J. Kulisch, T. Adermann, S. Passerini, Development of an all-solid-state lithium battery by slurry-coating procedures using a sulfidic electrolyte, Energy Storage Mater. 17 (2019) 204–210, https://doi.org/10.1016/j.ensm.2018.11.011.
[29] S. Chen, D. Xie, G. Liu, J.P. Mwizerwa, Q. Zhang, Y. Zhao, X. Xu, X. Yao, Sulfide solid electrolytes for all-solid-state lithium batteries: Structure, conductivity, stability and application, Energy Storage Mater. 14 (2018) 58–74, https://doi.org/10.1016/j.ensm.2018.02.020.
[30] D. Cao, Q. Li, X. Sun, Y. Wang, X. Zhao, E. Cakmak, W. Liang, A. Anderson, S. Ozcan, H. Zhu, Amphipathic Binder Integrating Ultrathin and Highly Ion-Conductive Sulfide Membrane for Cell-Level High-Energy-Density All-Solid-State Batteries, Adv. Mater. 33 (2021) 2105505, https://doi.org/10.1002/adma.202105505.

[31] B. Emley, Y. Liang, R. Chen, C. Wu, M. Pan, Z. Fan, Y. Yao, On the quality of tape-cast thin films of sulfide electrolytes for solid-state batteries, Mater. Today Phys. 18 (2021), 100397, https://doi.org/10.1016/j.mtphys.2021.100397.
[32] T.Y. Kwon, K.T. Kim, D.Y. Oh, Y.B. Song, S. Jun, Y.S. Jung, Three-dimensional networking binders prepared in situ during wet-slurry process for all-solid-state batteries operating under low external pressure, Energy Storage Mater. 49 (2022) 219–226, https://doi.org/10.1016/j.ensm.2022.04.017.
[33] R. Koerver, I. Aygün, T. Leichtweiß, C. Dietrich, W. Zhang, J.O. Binder, P. Hartmann, W.G. Zeier, J. Janek, Capacity Fade in Solid-State Batteries: Interphase Formation and Chemomechanical Processes in Nickel-Rich Layered Oxide Cathodes and Lithium Thiophosphate Solid Electrolytes, Chem. Mater. 29 (2017) 5574–5582, https://doi.org/10.1021/acs.chemmater.7b00931.
[34] J. Lee, K. Lee, T. Lee, H. Kim, K. Kim, W. Cho, A. Coskun, K. Char, J.W. Choi, In Situ Deprotection of Polymeric Binders for Solution-Processible Sulfide-Based All-Solid-State Batteries, Adv. Mater. 32 (2020) 2001702, https://doi.org/10.1002/adma.202001702.
[35] F. Hippauf, B. Schumm, S. Doerfler, H. Althues, S. Fujiki, T. Shiratsuchi, T. Tsujimura, Y. Aihara, S. Kaskel, Overcoming binder limitations of sheet-type solid-state cathodes using a solvent-free dry-film approach, Energy Storage Mater. 21 (2019) 390–398, https://doi.org/10.1016/j.ensm.2019.05.033.
[36] S. Cangaz, F. Hippauf, F.S. Reuter, S. Doerfler, T. Abendroth, H. Althues, S. Kaskel, Enabling High-Energy Solid-State Batteries with Stable Anode Interphase by the Use of Columnar Silicon Anodes, Adv. Energy Mater. 10 (2020) 2001320, https://doi.org/10.1002/aenm.202001320.
[37] T. Jiang, P. He, Y. Liang, L.-Z. Fan, All-dry synthesis of self-supporting thin Li10GeP2S12 membrane and interface engineering for solid state lithium metal batteries, Chem. Eng. J. 421 (2021), 129965, https://doi.org/10.1016/j.cej.2021.129965.
[38] K. Lee, S. Kim, J. Park, S.H. Park, A. Coskun, D.S. Jung, W. Cho, J.W. Choi, Selection of Binder and Solvent for Solution-Processed All-Solid-State Battery, J. Electrochem. Soc. 164 (2017) A2075–A2081, https://doi.org/10.1149/2.1341709jes.
[39] M. Yamamoto, Y. Terauchi, A. Sakuda, M. Takahashi, Binder-free sheet-type all-solid-state batteries with enhanced rate capabilities and high energy densities, Sci. Rep. 8 (2018) 1212, https://doi.org/10.1038/s41598-018-19398-8.
[40] K.T. Kim, D.Y. Oh, S. Jun, Y.B. Song, T.Y. Kwon, Y. Han, Y.S. Jung, Tailoring Slurries Using Cosolvents and Li Salt Targeting Practical All-Solid-State Batteries Employing Sulfide Solid Electrolytes, Adv. Energy Mater. 11 (2021) 2003766, https://doi.org/10.1002/aenm.202003766.
[41] D.Y. Oh, K.T. Kim, S.H. Jung, D.H. Kim, S. Jun, S. Jeoung, H.R. Moon, Y.S. Jung, Tactical hybrids of Li+-conductive dry polymer electrolytes with sulfide solid electrolytes: Toward practical all-solid-state batteries with wider temperature operability, Mater. Today 53 (2021) 7–15, https://doi.org/10.1016/j.mattod.2021.01.006.
[42] J. Ruhl, L.M. Riegger, M. Ghidiu, W.G. Zeier, Impact of Solvent Treatment of the Superionic Argyrodite Li6PS5Cl on Solid-State Battery Performance, Adv. Energy Sustain. Res. 2 (2021) 2000077, https://doi.org/10.1002/aesr.202000077.
[43] H. Muramatsu, A. Hayashi, T. Ohtomo, S. Hama, M. Tatsumisago, Structural change of Li2S–P2S5 sulfide solid electrolytes in the atmosphere, Solid State Ion. 182 (2011) 116–119, https://doi.org/10.1016/j.ssi.2010.10.013.
[44] W. Cho, J. Park, K. Kim, J.-S. Yu, G. Jeong, Sulfide-Compatible Conductive and Adhesive Glue-Like Interphase Engineering for Sheet-Type All-Solid-State Battery, Small 17 (2021) 1902138, https://doi.org/10.1002/smll.201902138.
[45] K. Chen, S. Shinjo, A. Sakuda, K. Yamamoto, T. Uchiyama, K. Kuratani, T. Takeuchi, Y. Orikasa, A. Hayashi, M. Tatsumisago, Y. Kimura, T. Nakamura, K. Amezawa, Y. Uchimoto, Morphological Effect on Reaction Distribution Influenced by Binder Materials in Composite Electrodes for Sheet-type All-Solid-State Lithium-Ion Batteries with the Sulfide-based Solid Electrolyte, J. Phys. Chem. C 123 (2019) 3292–3298, https://doi.org/10.1021/acs.jpcc.8b09569.
[46] M. Yamamoto, M. Takahashi, Y. Terauchi, Y. Kobayashi, S. Ikeda, A. Sakuda, Fabrication of composite positive electrode sheet with high active material content and effect of fabrication pressure for all-solid-state battery, J. Ceram. Soc. Jpn. 125 (2017) 391–395, https://doi.org/10.2109/jcersj2.16321.
[47] D.Y. Oh, D.H. Kim, S.H. Jung, J.-G. Han, N.-S. Choi, Y.S. Jung, Single-step wet-chemical fabrication of sheet-type electrodes from solid-electrolyte precursors for all-solid-state lithium-ion batteries, J. Mater. Chem. A 5 (2017) 20771–20779, https://doi.org/10.1039/C7TA06873E.
[48] S. Wang, X. Zhang, S. Liu, C. Xin, C. Xue, F. Richter, L. Li, L. Fan, Y. Lin, Y. Shen, J. Janek, C.-W. Nan, High-conductivity free-standing Li6PS5Cl/poly(vinylidene difluoride) composite solid electrolyte membranes for lithium-ion batteries, J. Materiomics 6 (2020) 70–76, https://doi.org/10.1016/j.jmat.2019.12.010.
[49] L. Cong, Y. Li, W. Lu, J. Jie, Y. Liu, L. Sun, H. Xie, Unlocking the Poly(vinylidene fluoride-co-hexafluoropropylene)/Li10GeP2S12 composite solid-state Electrolytes for Dendrite-Free Li metal batteries assisting with perfluoropolyethers as bifunctional adjuvant, J. Power Sources 446 (2020), 227365, https://doi.org/10.1016/j.jpowsour.2019.227365.
[50] S. Sen, E. Trevisanello, E. Niemöller, B.-X. Shi, F.J. Simon, F.H. Richter, The role of polymers in lithium solid-state batteries with inorganic solid electrolytes, J. Mater. Chem. A 9 (2021) 18701–18732, https://doi.org/10.1039/D1TA02796D.
[51] J. Xu, S.-L. Chou, Q.-F. Gu, H.-K. Liu, S.-X. Dou, The effect of different binders on electrochemical properties of LiNi1/3Mn1/3Co1/3O2 cathode material in lithium ion batteries, J. Power Sources 225 (2013) 172–178, https://doi.org/10.1016/j.jpowsour.2012.10.033.
[52] Z. Zhang, T. Zeng, Y. Lai, M. Jia, J. Li, A comparative study of different binders and their effects on electrochemical properties of LiMn2O4 cathode in lithium ion batteries, J. Power Sources 247 (2014) 1–8, https://doi.org/10.1016/j.jpowsour.2013.08.051.
[53] D.Y. Oh, Y.J. Nam, K.H. Park, S.H. Jung, K.T. Kim, A.R. Ha, Y.S. Jung, Slurry-Fabricable Li^+-Conductive Polymeric Binders for Practical All-Solid-State Lithium-Ion Batteries Enabled by Solvate Ionic Liquids, Adv. Energy Mater. 9 (2019) 1802927, https://doi.org/10.1002/aenm.201802927.
[54] M. Yamamoto, Y. Terauchi, A. Sakuda, M. Takahashi, Slurry mixing for fabricating silicon-composite electrodes in all-solid-state batteries with high areal capacity and cycling stability, J. Power Sources 402 (2018) 506–512, https://doi.org/10.1016/j.jpowsour.2018.09.070.
[55] S. Jaiser, M. Müller, M. Baunach, W. Bauer, P. Scharfer, W. Schabel, Investigation of film solidification and binder migration during drying of Li-Ion battery anodes, J. Power Sources 318 (2016) 210–219, https://doi.org/10.1016/j.jpowsour.2016.04.018.
[56] M. Müller, L. Pfaffmann, S. Jaiser, M. Baunach, V. Trouillet, F. Scheiba, P. Scharfer, W. Schabel, W. Bauer, Investigation of binder distribution in graphite anodes for lithium-ion batteries, J. Power Sources 340 (2017) 1–5, https://doi.org/10.1016/j.jpowsour.2016.11.051.
[57] S. Kim, J. Chen, T. Cheng, A. Gindulyte, J. He, S. He, Q. Li, B.A. Shoemaker, P. A. Thiessen, B. Yu, L. Zaslavsky, J. Zhang, E.E. Bolton, PubChem in 2021: new data content and improved web interfaces, Nucleic Acids Res. 49 (2021) D1388–D1395, https://doi.org/10.1093/nar/gkaa971.
[58] Y. Ma, J. Ma, G. Cui, Small things make big deal: Powerful binders of lithium batteries and post-lithium batteries, Energy Storage Mater. 20 (2019) 146–175, https://doi.org/10.1016/j.ensm.2018.11.013.
[59] E.B. Twum, E.F. McCord, P.A. Fox, D.F. Lyons, P.L. Rinaldi, Characterization of Backbone Structures in Poly(vinylidene fluoride-co-hexafluoropropylene) Copolymers by Multidimensional 19F NMR Spectroscopy, Macromolecules 46 (2013) 4892–4908, https://doi.org/10.1021/ma400683w.
[60] Y.J. Nam, S.-J. Cho, D.Y. Oh, J.-M. Lim, S.Y. Kim, J.H. Song, Y.-G. Lee, S.-Y. Lee, Y. S. Jung, Bendable and Thin Sulfide Solid Electrolyte Film: A New Electrolyte Opportunity for Free-Standing and Stackable High-Energy All-Solid-State Lithium-Ion Batteries, Nano Lett. 15 (2015) 3317–3323, https://doi.org/10.1021/acs.nanolett.5b00538.